



Article

Multistage Evolution in Transverse Aeolian Ridges

Timothy Nagle-McNaughton * and Louis Scuderi

Department of Earth and Planetary Science, The University of New Mexico, Northrop Hall MSC03 2040, 221 Yale Boulevard Northeast, Albuquerque, NM 87131, USA; tree@unm.edu

* Correspondence: timnagle@unm.edu

Abstract: Transverse aeolian ridges (TARs) are poorly understood relict aeolian Martian surface features. Processes that create TARs are not well-constrained, and understanding their formation is complicated since they appear to share some features of ripples, megaripples, and dunes. While some evidence of multi-stage TAR formation has been documented in Nirgal Vallis, here we present additional evidence for this process at nine locations on Mars using cratering superposition between different ridge morphologies. Most occurrences of multistage evolution will not preserve the precise series of cratering and formation events documented here, which potentially means that this formative process may have been more common than even these new widespread observations suggest. This formative process can help determine the relative similarity of TARs to ripples, megaripples and dunes. Based on our observations, we conclude that primary TAR forms are most like megaripples, and that subsequent ridges formed like aqueous ripple spurs.

Keywords: transverse aeolian ridges; TARs; ripples; dunes; Martian surface



Citation: Nagle-McNaughton, T.; Scuderi, L. Multistage Evolution in Transverse Aeolian Ridges. *Remote Sens.* **2021**, *13*, 1329. <https://doi.org/10.3390/rs13071329>

Academic Editor: Kjartan Kinch

Received: 10 February 2021

Accepted: 24 March 2021

Published: 31 March 2021

Publisher's Note: MDPI stays neutral with regard to jurisdictional claims in published maps and institutional affiliations.



Copyright: © 2021 by the authors. Licensee MDPI, Basel, Switzerland. This article is an open access article distributed under the terms and conditions of the Creative Commons Attribution (CC BY) license (<https://creativecommons.org/licenses/by/4.0/>).

1. Introduction

1.1. Transverse Aeolian Ridges

Transverse aeolian ridges (TARs), first detected in narrow-angle images from the Mars Orbiter Camera (MOC), are bright linear landforms thought to be relict aeolian features [1–3]. While TARs are widespread on Mars, their role in past Martian sediment cycles is poorly understood [2–7]. While a recent study has suggested that some isolated TARs may be active [8], research suggests that the overwhelming majority of TARs are immobile with little evidence of interaction with current Martian winds [9–12].

TARs are sparse but common features across the surface of Mars [3] and display a range of sizes and forms (simple, forked, sinuous, barchan-like, deltoid, and networked) [2,6]. TAR morphologies are typically categorized by a single primary ridge crest, but secondary ridge crests have also been observed [2,13,14]. These secondary ridges remain largely unexplained [2,3,14], however they display similarities to raked linear dunes [15,16]. These secondary ridges may provide insights into TAR formative processes and evolution.

TARs share characteristics of both ripples and dunes. They are relatively symmetrical in profile [17,18], similar to wind ripples or reversing dunes. However, they can be much larger than wind ripples observed on Mars and Earth with wavelengths on the order of tens of meters [19–21], and appear to form in locations not conducive to reversing wind patterns.

Significant effort has been expended in attempts to identify TAR proxies on Earth: gravel megaripples in Argentina [22,23], megaripples in Iran and Libya [24–26], and reversing dunes in Idaho [27]. Despite these efforts, a definitive analog has not been established. A growing body of evidence suggests that TARs may be a form of megaripple [8,28–33], at the very least placing TARs closer to ripples on the ripple-dune continuum.

1.2. Aeolian Processes

As first laid out in Bagnold's 1941 seminal work, there are three general modes of aeolian sediment transport: suspension, saltation, and creep [34]. Suspension and saltation

occur within the boundary layer and, while not directly caused by wind, creep occurs in the laminar sublayer if one is present. Of these processes, saltation is responsible for the vast majority of aeolian sediment transport on Earth, as much as 95% by some estimates [35,36].

While it is clear that ripples and dunes can be easily differentiated by their obvious morphological differences, a more important distinction is that the two can be separated with respect to their role within the aeolian sediment cycle. Dunes exert an influence on local sediment transport rates through flow-form interactions induced by the topography of the dune itself [34,37–40]. The topographic disturbance created by a dune is responsible for airflow acceleration and deceleration [41–44], and can generate new structures within the airflow [45–52]. Further, airflow on the lee side of dunes separates from the topography, before eventually reattaching [53–56]. These complex dynamics result in a range of dune morphologies, migration patterns and rates, and evolutionary paths, which each represent some stasis between dunes, sediment supply, and wind conditions [57–60]. These conditions may not be permanent (i.e., a disequilibrium, or threshold/feedback non-equilibrium [61]) but can be sustained for over time-scales that allow these conditions to be captured in the sedimentological record enabling insight into past conditions [62–68].

Wind ripples are simpler forms, generally forming perpendicular to the prevailing winds, with some influence from slope [69,70]. Unlike dunes, ripples do not cause flow separation or eddies and merely respond to airflow without meaningfully altering it [34,69–71]. Ripples are commonly found on sand dunes, illustrating disparate erosional and depositional processes at work simultaneously. Further, unlike dunes, ripples form and change quickly and represent a nearly instantaneous record of local sediment transport and wind direction [35]. On Mars, ripples tend to have wavelengths of 0.1–3 m, with amplitudes of a few decimeters, and tend to be dark toned. Megaripples are a related form of wind ripples that are of greater size and wavelength (amplitudes of a couple of meters, and wavelengths in the low tens of meters) that are dominated by reptation and creep [28,30,34,69,72]. While normal ripples typically form in areas with uniform sand grain size, megaripples tend to be found in areas with both coarse sand and bimodal grain-size distributions [23,28,34,69,72–77].

Like dunes, sand megaripples on Earth have been documented with some ripple mantling [25,72,78], indicative of at least a semi separate formative process. While both ripples and megaripples typically have the coarsest grains at their crests, megaripples tend to have larger grains overall, making them especially wind resistant [69,72,74,75,77,79,80]. Thus, relative to both dunes and ripples, megaripple migration is significantly slower [28,31,78,80]. Long term studies of megaripples are rare, but the literature suggests that since they are comparatively immobile and respond only to the strongest wind flows, they could thus represent records of extreme wind events [31,73,75–78,81–83]. There is conflicting evidence for this large-grain mantle on TARs: examination of TAR thermal inertias suggest that TARs are covered by smaller grains than dunes at least on the surface [84,85]. Taking this into account, a cemented dust/ice mantle hypothesis has been proposed to explain the inactivity of TARs [2]. However, a recent study using in situ observations from the Curiosity rover suggested that a relatively small TAR in Dingo Gap should be considered a megaripple due to a mantling of large grains too massive to be activated by saltation [32].

Despite the differences outlined above, aeolian features lie on a continuum that at times does not lend itself to easy discrimination of between classes. Ripples, megaripples, and TARs can all overlap in terms of their amplitude and wavelength on Mars [86]. For example, such a grey area occurs between active ripples and inactive coarse-grained ripples [87,88], between large ripples and small TARs [5,31], and between active megaripples and small TARs [8,89,90]. These are problematic since formative mechanisms can be difficult to distinguish when features share characteristic wavelengths [33]. For the purposes clarity, we will employ the following definitions: ripples are saltation-dominated features with wavelengths of a few meters at most; megaripples are less mobile, dominated by creep and reptation, have wavelengths of a few tens of meters and amplitudes measured in meters; TARs are minimally active bright bedforms with wavelengths of tens of meters, and dunes

are simply much larger features overall with wavelengths on the order of hundreds of meters.

1.3. Multi-Stage TAR Formation and This Study

Cratering in superposition between TARs of different scales and orientations has been documented in Nirgal Vallis [14]. This cratering suggests an evolutionary sequence of TAR development. Figure 1 shows the proposed general sequence [14]. Here, we present previously undocumented evidence of multi-stage TAR formation, and discuss possible mechanisms in relation to other aeolian processes.

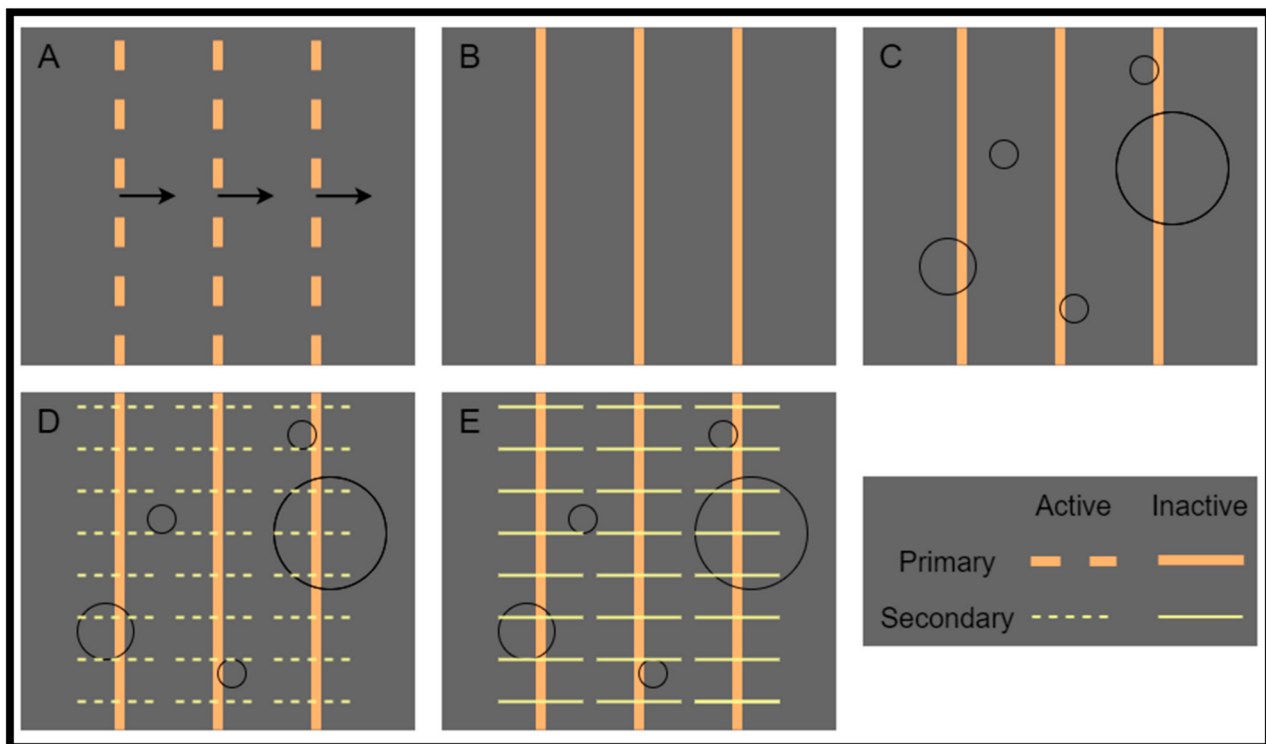


Figure 1. TAR evolution. (A) Initial TARs form and are active; (B) The initial TARs are stabilized and/or cemented; (C) The initial TARs remain preserved for a significant period (as shown by cratering); (D) Secondary TARs with morphologies that differ the first form; (E) These secondary TARs also become stabilized. Note the superposition in 5: cratering over the primary TARs, and secondary TARs over the craters.

2. Materials and Methods

Thirty High Resolution Imaging Science Experiment (HiRISE) images [91] were downloaded (Appendix A) and examined for cratering suggestive of multigenerational TARs (as shown in Figure 1). Craters of interest were determined by the following sequence:

1. Identify impact craters.
2. Delineate any overlap with TAR crests.
3. Determine whether TAR crests predate or postdate the impact.
4. Determine whether there was subsequent modification of the crater by different aeolian features.

To determine the age relationships between TARs and craters within the TAR field in step 3, we analyzed a number of spatial relationships (Figure 2). We classed TARs as predating the craters if one or more of the following criteria were met: (A) The crater deformed the ridge-crest, indicating that the ridge was altered after formation. (B) TARs narrow at either end so a relatively wide TAR terminating at a crater likely did not naturally terminate there, (C) The crater completely interrupts the ridge-crest, (D) The crater rim is obviously taller than intersecting TARs and is clearly superimposed over nearby TARs.

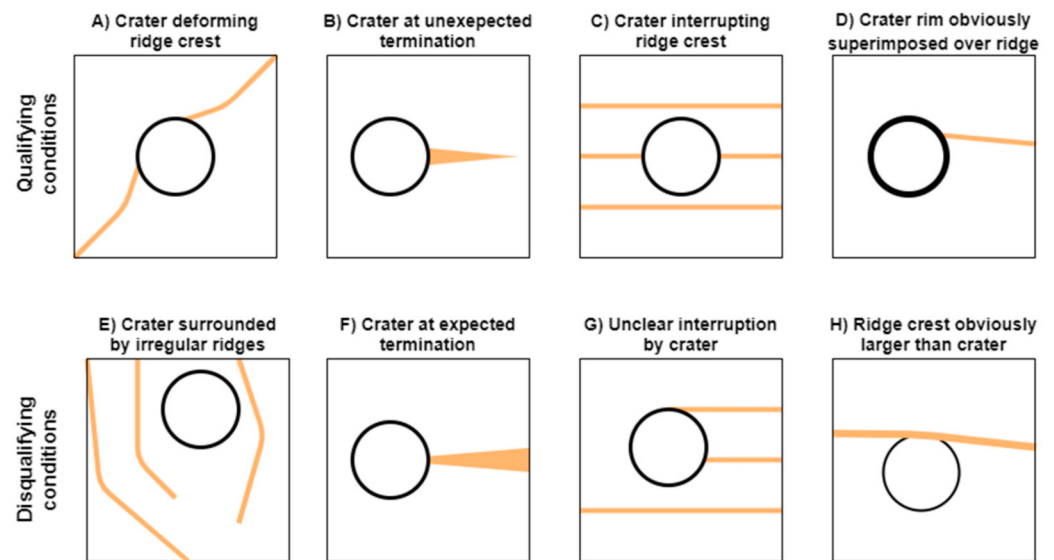


Figure 2. Diagrammatic examples of interactions between TAR crests (orange) and craters (black circles). See text for details.

Alternatively, TARs were classified as post-dating the craters, or of indeterminate age relative to the TARs, if any of the following conditions were met (Figure 2): (E) the TARs that intersect the crater were too irregular or sparse to determine interruption or interaction, (F) Intersecting TARs narrow towards the crater rim, potentially indicating a natural termination, (G) the TARs lacked obvious corresponding ridges on the other side of the crater, precluding any determination of interruption and potentially indicative of a natural termination, (H) the TARs had amplitudes that were greater than the height of the crater rim, suggesting that any alteration of the ridge crest could be from the topographic disturbance of the preexisting rim.

TARs in images with evidence for multi-stage formation were characterized by their primary features (width, length, and orientation) [2], and these metrics and traced crestlines were documented in ArcGIS Pro databases [92].

3. Results

3.1. Cratering Superposition

Evidence for multi-stage TAR formation with up to three distinct TAR morphologies was found in nine of the 30 HiRISE images (Table 1). Examples of 16 such previously undocumented occurrences are shown in Figure 3. Crater modification was more common in areas where the TARs were large, and long, and relatively simple. Crater-modifying TARs were relatively small, but were larger and more complex than typical ripples (Figure 3). These modifying features had variable orientations, sometimes perpendicular to the underlying larger TARs, and were typically more sinuous than their larger counterparts.

Table 1. HiRISE imagery used in TAR interaction studies.

HiRISE Image	Resolution (m/pixel)	Crater Example Number(s) in Figures 3 and 4
ESP_015894_1545	0.25	C, N, O
ESP_017661_1545	0.50	B
ESP_027708_1815	0.25	A
ESP_055374_1510	0.50	D
ESP_064877_1670	0.25	E
ESP_065169_2085	0.50	J
ESP_065223_1855	0.25	G
ESP_065260_1715	0.25	H
PSP_010448_1530	0.25	F, I, K, L, M, P

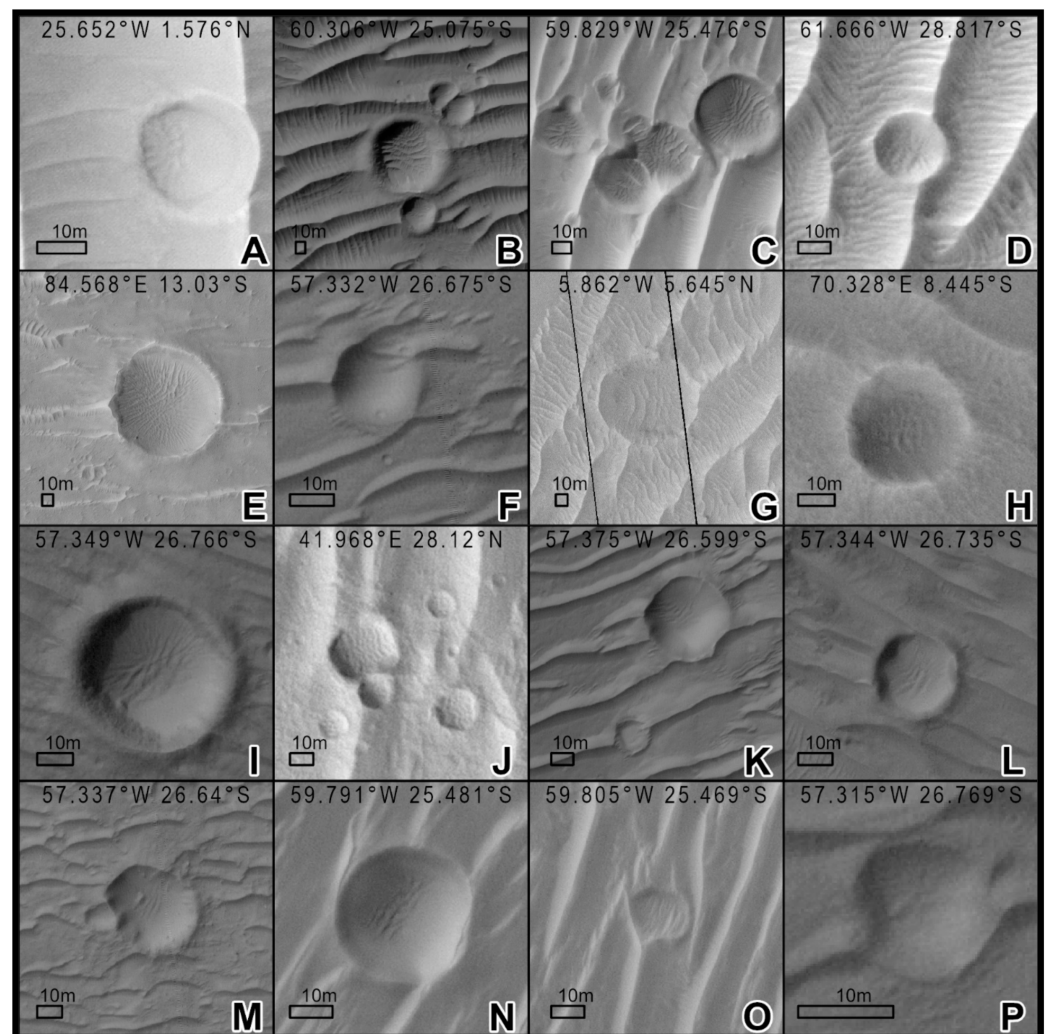


Figure 3. A selection of modified craters. Note that many of the most well-developed modifying ridges are either larger or more complex than ripples (notably B, C, E, F, G, and O). Coordinates mark the center of each image, and north is up in these and all following images. See Table 1 for image details.

Cratering over TARs is rare, and modification of these craters is even more uncommon: most craters in TARs showed no encroachment of secondary features, even among craters with comparable size, states of rim-preservation, and in the same general locations. For

example, many of these unmodified craters (Figure 4) are located in close proximity to corresponding numbered modified craters shown in Figure 3 (in some cases within meters).

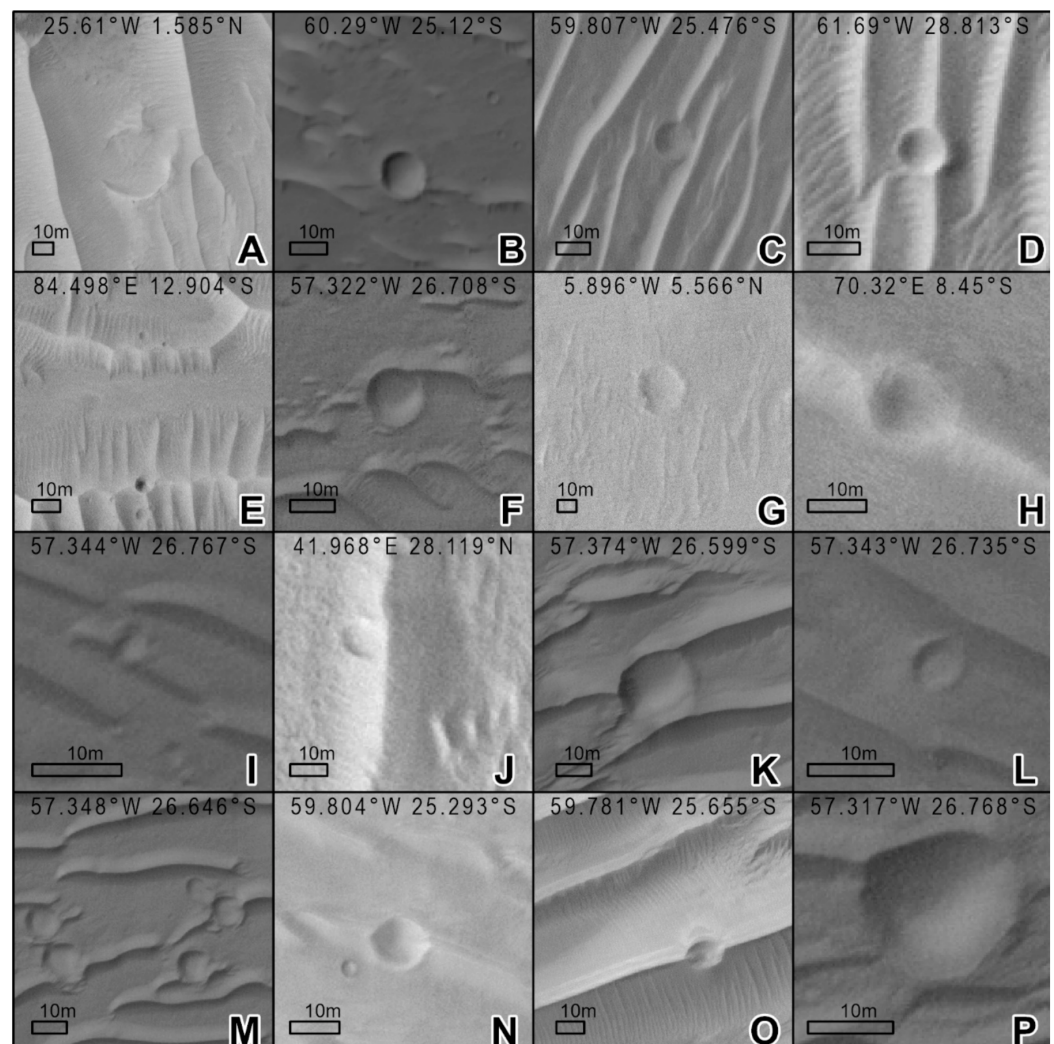


Figure 4. A selection of craters in TARs without subsequent ridge development. Note range of scales in the TAR and crater sizes. Most of the craters have likely experienced post-impact infilling (see A and H). Coordinates mark the center of each image. See Table 1 for image sources.

3.2. Ridge Morphologies

In areas with confirmed cratering in superposition between ridge morphologies, up to three different morphologies were identified (Figure 5, Table 2). We characterize these features as follows; **Feature 1:** Primary TARs with large bright ridges with wavelengths of tens of meters. They generally have simple crest morphologies with very limited sinuosity and forking. **Feature 2:** Secondary ridges, small crests typically appearing on the flanks of the primary ridges. These ridges intersect primary TARs at angles between 60° and 90°. While the wavelengths of these ridges are variable, it usually is <10 m. These ridges have similarly simple crest morphologies that have been noted in previous studies [2,11,93], but have not been well documented. The length of these secondary ridges is limited to a few meters. **Feature 3:** Tertiary ridges, even smaller than secondary ridges, located in turn on the flanks of some secondary ridges. Tertiary ridges are usually only 1 m in length, and have wavelengths of a few meters. They can be difficult to identify given their scale is at the limits of the HiRISE data. These ridges have only been noted since the widespread dissemination and examination of HiRISE imagery [11], but are more poorly documented

than secondary ridges. Tertiary ridges have essentially simple crest morphologies, but defects may be masked by resolution limitations.

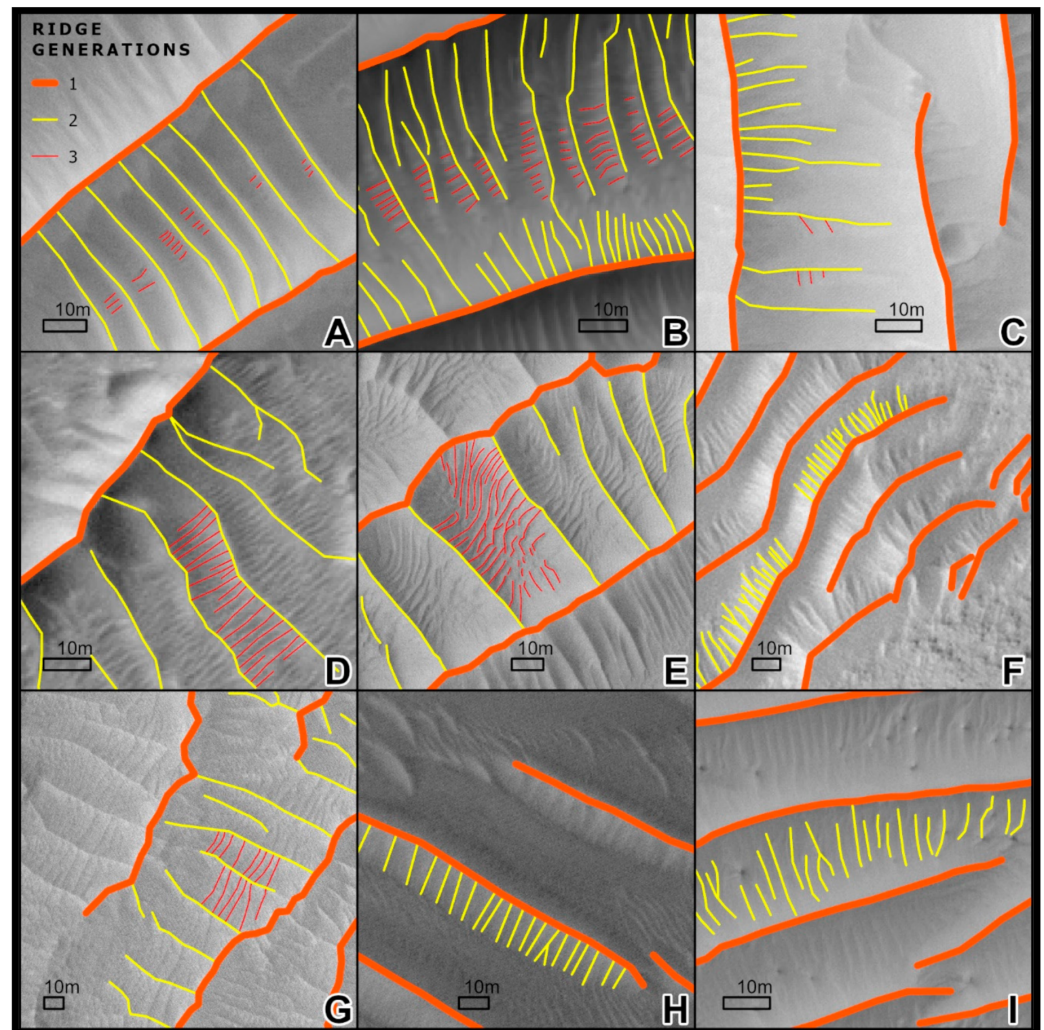


Figure 5. Manually traced ridge morphologies. Thick orange lines represent Primary TARs, thinner yellow lines Secondary ridges, and thin red lines Tertiary ridges. Note the near-perpendicular offsets between each ridge morphology. Coordinates mark the center of each image. See Table 2 for details.

Secondary ridges are more common on very large simple TARs. The size of these secondary ridges spans an order of magnitude, ranging in wavelength from 1 m (e.g., the south side of Site B in Figure 5), to over 25 m (e.g., Sites E and G in Figure 5). Secondary ridges generally scale in length and width with primary TARs, but the ratio of primary to secondary wavelengths is highly variable, ranging from 3–10. Tertiary ridges were only observed on very large simple TARs, however, not enough were documented to reach general conclusions about their wavelength relationships. Where tertiary ridges were best developed (e.g., Sites B, D, G in Figure 5) the ratio of secondary to tertiary wavelength, like the primary secondary ratio, is 3–10.

Table 2. Observed ridge morphologies in Figure 5, all measurements in meters.

Annotated Example	HiRISE Observation	Primary Ridges			Secondary Ridges			Tertiary Ridges		
		Width (m)	Length (m)	Wavelength (m)	Width (m)	Length (m)	Wavelength (m)	Width (m)	Length (m)	Wavelength (m)
A	ESP_015894_1545	100–500	20–40	35–70	30–60	3–5	8–12	2–4	<1	1–3
B	ESP_017661_1545	100–1000	25–40	20–60	35–50	1–4	2–9	1–4	1	1–3
C	ESP_027708_1815	80–300	25–35	25–50	15–30	1–2	4–12	1–2	<1	3–4
D	ESP_055374_1510	80–160	12–30	70–90	40–90	2–6	7–15	3–15	1	1–3
E	ESP_064877_1670	80–170	15–30	40–70	25–50	4–8	8–30	3–30	1	2–4
F	ESP_065169_2085	15–190	15–20	20–25	5–15	1–2	2–6	–	–	–
G	ESP_065223_1855	60–250	15–25	25–80	15–80	2–4	10–25	10–25	<1	3–8
H	ESP_065260_1715	40–150	10–25	15–55	8–15	1–2	5–10	–	–	–
I	PSP_010448_1530	30–250	10–20	20–30	5–20	1–2	2–5	–	–	–

4. Discussion

4.1. Uncertainty in Determining Crater Superposition

TARs illustrate a degree of topographic control [2], and this can make interpreting TAR-crater interactions difficult. For example, in each image in Figure 6, there could be two possible explanations: (1) The TAR predates the crater: The original TAR was impacted, deflected, and reformed under the influence of the new crater, or (2) The crater predates the TAR: the topographic disturbance of the crater and crater rim influenced the initial formation of the TAR. This pattern is common (Figure 6). Thus, it is important to treat any potential example with reasonable skepticism. In Figure 4, we presented some of the best examples from our survey, but without definitive ground-based imagery, there remains a degree of uncertainty in our assessments.

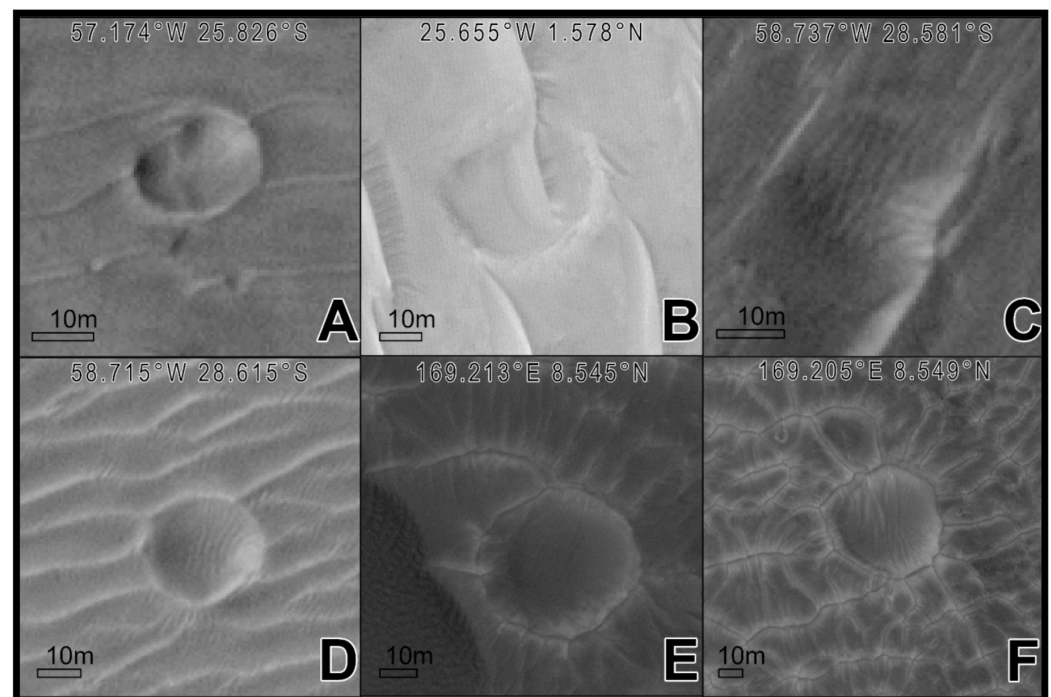


Figure 6. Ambiguous TAR-crater relationships where the superpositioning is indeterminate. (A) The TAR at the top of the crater appears to bend along the edge of the crater, while both the TAR on the left and the lower TAR on the right have ambiguous intersections with the crater rim. (ESP_047726_1540)

(B) The TAR at the top of the image appears to be deflected left by the crater rim. This could be the effect of the preexisting crater, or a result of post-impact reactivation (ESP_027708_1815) (C) The large bright TAR appears to be deformed and bent by the left by the faint crater. (ESP_031256_1510) (D) The TARs at the top and bottom of the crater appear to bend around the crater rim, and the middle TAR on the left has an ambiguous intersection with the crater rim. (ESP_031256_1510) (E) The crater is entirely ringed by what appear to be extensions of the ridge to the upper left. The intersecting ridges surrounding the crater could have already existed and have been reactivated by the impact, or could they be entirely post-impact features (ESP_067037_1885) (F) Like (E), this crater appears to both interrupt pre-existing ridges (e.g., the long ridge intersecting the lower left), while also generating other ridges due to its topographic disturbance (such as the series extending perpendicularly from the ridge clockwise from the top). (ESP_067037_1885) Coordinates mark the center of each image.

4.2. The Timing between Generations of Ridges

Cratering between different ridge morphologies is suggestive of multiple generations of ridge formation. The presence of craters on top of large TARs shows that the TARs predate the craters. Based on the absence of craters on active dune bedforms on Mars, we conclude that the TARs were immobilized or stabilized before impact. If TARs have been significantly mobile or active since, the crater rims should show alteration/degradation, but most crater rims were relatively clear for impacts in aeolian sediment. Post-cratering, the disparate morphologies of the intra-crater features indicate that a second period of ridge formation occurred. These secondary ridges appear to also have been preserved like the larger TARs, and have not been detectibly active.

The formation of the second generation of ridges is not universal. As noted previously, presence or absence of intra-crater ridges can vary over even just a few tens of meters. There is little reason to doubt that the formation of complex morphologies by multiple ridge generations is a localized phenomenon and likely occurred across Mars. We propose that secondary ridges likely represent a subsequent generation of bedforms (rather than features that developed simultaneously with the primary TARs) and that the tertiary ridges probably formed sometime after the stabilization of the secondary ridges. We hypothesize that this series of events likely occurred elsewhere on Mars even where crater superpositioning cannot be conclusively used to determine relative ages.

4.3. TAR Analogs and Implications

Here, we explore possible mechanisms for multigenerational TAR formation, and discuss what relationships between these primary, secondary, and tertiary ridges imply. Broadly, there are three distinct lenses for examining TAR formation: dune-like, megaripple-like, and ripple-like. While there is limited evidence for each process, we note that the megaripple hypothesis has gained recent support [33].

Dunes offer poor alternative formation mechanisms for secondary/tertiary ridges. While significant flow deflection has been observed over terrestrial dune crests [94,95], as has transport parallel to unidirectional dunes [51,56,96], both dune-crest flow alteration mechanisms require full flow separation and the development of lee-side vortices. This contradicts our observation of symmetrical secondary ridges on both sides of TARs [14], and is fundamentally at odds with the invocation of lee-side mechanisms, except in the case of reversing wind patterns. However, while TAR's display reversing dune type profiles [17,18,27,97], transverse dunes produce the best examples of flow deflection and secondary airflow on Earth.

Formation issues aside, the pattern of the secondary/tertiary ridges is also problematic through a dune lens. The perpendicular forms are comparable to the similar, but much larger, polygonal dune organization of Olympia Undae near the Martian north pole [98]. However, the patterns in these dunes were created by changes in wind direction [98], and winds that regularly shift by 90° are unlikely to be present everywhere the ~90° offset pattern in TAR ridges is observed. For example, primary ridges in the sinuous Nirgal Vallis

can easily be explained by flow channeled through the valley, but the secondary ridges would unrealistically require wind directions to vary very precisely in order to always flow perpendicularly across the valley, even as the valley twists and turns [14].

With respect to ripples, recent work suggests that the wind induced dynamic pressures on Mars could allow for ripple formation an order of magnitude large than those on Earth [33]. While there is some overlap between the scale of very large ripples on Mars and small TARs, geomorphically ripples are an unlikely analog for TARs. Ripples are highly responsive to changes in wind conditions, are transient and are still significantly active on Mars while TARs are minimally active over near-decadal periods [8]. Further, most secondary ripples documented on Mars are almost universally parallel to the main ridge crests [33,66], unlike the secondary ridges documented here.

Assuming that primary/secondary/tertiary ridge organization at least minimally represent separate generations, there are two obvious explanations for the perpendicular/oblique orientations of secondary/tertiary ridges: (1) primary TARs create localized change in airflow passing over the ridges via flow deflection and eddy/vortex formation, or (2) the larger regional wind patterns changed by 90° repeatedly. The latter explanation is less probable; as we noted above, changes in wind patterns—whether seasonal or otherwise—are unlikely to match the regularity of many of the secondary and tertiary ridge orientations, especially given how widespread the perpendicularity is. Additionally, the regularity and frequency of the 90° offset would appear to preclude this explanation.

The former possibility, that secondary/tertiary ridges are the result of localized alterations to the lower boundary layer caused by of flow deflection over main crest and some sort of secondary airflow in the troughs, is more plausible. Recent experiments have found secondary features can occur with ripples dubbed “bedform spurs” [99,100]. These features, created by vortices shed by ripples, appear in aqueous flows when ripples were ~25–90° offset from the flow direction [99,100]. Bedform spurs have a striking resemblance to the secondary/tertiary ridges, and have spacings well described by a linear relationship to the parent ridge scale, similar to the pattern documented in Table 2 [99]. Further, in some cases, spurs were frequently observed forming at a 90° offset to the main crest [100]: precisely to the pattern observed on Mars. Bedform spurs remain a promising avenue for further comparative study.

Megaripples are the most likely analog for the main TAR ridge crests given their scale and inactivity. Megaripples on Earth are relatively rare, and form under very specific conditions including but not limited to: erosive sorting, coarsening, coarse-grain reputation, as well as a precise range of wind conditions—with high velocities sufficient to mobilize coarse grains, but not so fast as to destroy or flatten the ripples [72,77,79,80]. However, on Mars the wind velocity required to flatten a megaripple the size of the observed TARs vastly exceeds local observations [33], meaning that TARs would only be erased under extreme conditions. Further, the lower wind pressures on Mars do not place the same finite upper limit on megaripple growth that exist on Earth, allowing megaripple scales to vary over a larger range than on Earth. This wide range of sizes is observed in TARs on Mars.

Based thus these observations we thus conclude the primary ridge crests most likely formed as outsized megaripples, and that the secondary ridges and tertiary ridges formed like ripple spurs which are produced by vortexes shed by the larger crests.

4.4. How Did TARs Form?

Maybe the most fundamental question about TARs does not have a definitive answer. Testing new hypotheses about TAR origins and development requires statistically valid samples covering the entire range of geomorphic morphologies and localities where they are found. Large databases of these morphologies, locations, elevations, and co-occurrences with other features (craters, dunes, etc.) would be an ideal starting point. While some manual surveys of TARs have been performed [1–3], recent work in the development of automated methods for identifying TARs [101] and other features will likely prove crucial to these efforts.

Furthermore, additional ground survey-based data would be useful for understanding TARs as well. While the Curiosity and Opportunity rovers have documented and even interacted some ripples and TARs [32,102] the data compiled from these observations are limited. Jezero Crater, the recent landing site of the Mars 2020 Perseverance rover [103], contains many TARs and will provide an excellent opportunity to obtain more in situ TAR data, which can be used to test some of the hypotheses identified in this paper.

5. Conclusions

Here, we present new evidence for the multi-stage formation of TARs on Mars using the superpositioning of craters within different aeolian ridge morphologies. Our observations suggest that multiple generations of activity created the more complex TAR forms we observe in our study areas. We found that this process was likely dependent on local wind conditions, with occurrences varying over a length-scale of a few tens of meters. We conclude that TARs form in the most similar manner to megaripples rather than ripples or dunes, and that, based on comparisons between secondary/tertiary ridges and ripples spurs, the later second and third generation ridges we observe are produced by vortices shed by the main ridge.

Author Contributions: Conceptualization, T.N.-M. and L.S.; methodology, T.N.-M.; formal analysis, T.N.-M. and L.S.; resources, L.S.; data curation, T.N.-M.; writing—original draft preparation, T.N.-M.; writing—review and editing, T.N.-M. and L.S.; visualization, T.N.-M.; supervision, L.S.; project administration, L.S.; funding acquisition, T.N.-M. and L.S. All authors have read and agreed to the published version of the manuscript.

Funding: This project was supported by NASA Doctoral Fellowship 80NSSC19K1676.

Data Availability Statement: All data used in this study are publicly available imagery.

Acknowledgments: The authors would like to thank the three anonymous reviewers for their help and patience in improving this manuscript.

Conflicts of Interest: The authors declare no conflict of interest.

Appendix A List of Examined Images

HiRISE Observation	Cratering in Superposition Observed
ESP_013071_1365	No
ESP_015894_1545	Yes
ESP_017661_1545	Yes
ESP_018186_1865	No
ESP_021688_1325	No
ESP_023817_1800	No
ESP_025622_1385	No
ESP_027687_2650	No
ESP_027708_1815	Yes
ESP_028297_1380	No
ESP_033460_1725	No
ESP_035514_2610	No
ESP_040559_1845	No
ESP_046465_2165	No
ESP_052179_2215	No
ESP_053339_1575	No
ESP_054690_1670	No

HiRISE Observation	Cratering in Superposition Observed
ESP_055374_1510	Yes
ESP_056216_2185	No
ESP_056777_0925	No
ESP_058373_1355	No
ESP_062483_1755	No
ESP_064851_1675	No
ESP_064877_1670	Yes
ESP_065169_2085	Yes
ESP_065223_1855	Yes
ESP_065260_1715	Yes
ESP_065853_1190	No
PSP_010448_1530	Yes
ESP_013071_1365	No

References

- Wilson, S.A.; Zimbelman, J.R. Latitude-Dependent Nature and Physical Characteristics of Transverse Aeolian Ridges on Mars. *J. Geophys. Res. E Planets* **2004**, *109*, 1–12. [[CrossRef](#)]
- Balme, M.; Berman, D.C.; Bourke, M.C.; Zimbelman, J.R. Transverse Aeolian Ridges (TARs) on Mars. *Geomorphology* **2008**, *101*, 703–720. [[CrossRef](#)]
- Berman, D.C.; Balme, M.R.; Rafkin, S.C.R.; Zimbelman, J.R. Transverse Aeolian Ridges (TARs) on Mars II: Distributions, Orientations, and Ages. *Icarus* **2011**, *213*, 116–130. [[CrossRef](#)]
- Chojnacki, M.; Hargitai, H.; Kereszturi, Á. Encyclopedia of Planetary Landforms. *Encycl. Planet. Landf.* **2015**, 1–6. [[CrossRef](#)]
- Geissler, P.E.; Wilgus, J.T. The Morphology of Transverse Aeolian Ridges on Mars. *Aeolian Res.* **2017**, *26*, 63–71. [[CrossRef](#)]
- Geissler, P.E. The Birth and Death of Transverse Aeolian Ridges on Mars. *J. Geophys. Res. Planets* **2014**, 2583–2599. [[CrossRef](#)]
- Bridges, N.T.; Bourke, M.C.; Geissler, P.E.; Banks, M.E.; Colon, C.; Diniega, S.; Golombek, M.P.; Hansen, C.J.; Mattson, S.; McEwen, A.S.; et al. Planet-Wide Sand Motion on Mars. *Geology* **2012**, *40*, 31–34. [[CrossRef](#)]
- Silvestro, S.; Chojnacki, M.; Vaz, D.A.; Cardinale, M.; Yizhaq, H.; Esposito, F. Megaripple Migration on Mars. *J. Geophys. Res. Planets* **2020**. [[CrossRef](#)]
- Fenton, L.K.; Bandfield, J.L.; Ward, A.W. Aeolian Processes in Proctor Crater on Mars: Sedimentary History as Analyzed from Multiple Data Sets. *J. Geophys. Res. Planets* **2003**, *108*, 5129. [[CrossRef](#)]
- Bridges, N.; Geissler, P.; Silvestro, S.; Banks, M. Bedform Migration on Mars: Current Results and Future Plans. *Aeolian Res.* **2013**, *9*, 133–151. [[CrossRef](#)]
- Berman, D.C.; Balme, M.R.; Michalski, J.R.; Clark, S.C.; Joseph, E.C.S. High-Resolution Investigations of Transverse Aeolian Ridges on Mars. *Icarus* **2018**, *312*, 247–266. [[CrossRef](#)]
- Reiss, D.; van Gasselt, S.; Neukum, G.; Jaumann, R. Absolute Dune Ages and Implications for the Time of Formation of Gullies in Nirgal Vallis, Mars. *J. Geophys. Res. E Planets* **2004**, *109*, 1–9. [[CrossRef](#)]
- Ren, S.; Qin, Q.; Ren, H.; Sui, J.; Zhang, Y. Heat and Drought Stress Advanced Global Wheat Harvest Timing from 1981–2014. *Remote Sens.* **2019**, *11*, 971. [[CrossRef](#)]
- Nagle-McNaughton, T.P.; Scuderi, L.A. A Geomorphological Case for Multistage Evolution of Transverse Aeolian Ridges (TARs) in Nirgal Vallis. *Planet. Space Sci.* **2021**, 105192. [[CrossRef](#)]
- Dong, Z.; Wei, Z.; Qian, G.; Zhang, Z.; Luo, W.; Hu, G. “Raked” Linear Dunes in the Kumtagh Desert, China. *Geomorphology* **2010**, *123*, 122–128. [[CrossRef](#)]
- Lü, P.; Narteau, C.; Dong, Z.; Rozier, O.; Courrech Du Pont, S. Unravelling Raked Linear Dunes to Explain the Coexistence of Bedforms in Complex Dunefields. *Nat. Commun.* **2017**, *8*. [[CrossRef](#)] [[PubMed](#)]
- Zimbelman, J.R.; Williams, S.H. Dunes versus Ripples: Topographic Profiling across Terrestrial Examples, with Application to the Interpretation of Features on Mars. In *AGU 88 Abstract P34A-07*; American Geophysical Union: Washington, DC, USA, 2007.
- Shockey, K.M.; Zimbelman, J.R. Analysis of Transverse Aeolian Ridge Profiles Derived from HiRISE Images of Mars. *Earth Surf. Process. Landf.* **2013**, *38*, 179–182. [[CrossRef](#)]
- Bourke, M.C.; Balme, M.; Beyer, R.A.; Williams, K.K.; Zimbelman, J. A Comparison of Methods Used to Estimate the Height of Sand Dunes on Mars. *Geomorphology* **2006**, *81*, 440–452. [[CrossRef](#)]
- Wilson, S. Large Aeolian Ripples: Extrapolations from Earth to Mars. In Proceedings of the Lunar and Planetary Science Conference, March, TX, USA, 17–21 March 2003; pp. 1–2.
- Williams, S. Large Ripples on Earth and Mars. In Proceedings of the Lunar and Planetary Science Conference, League City, TX, USA, 11–15 March 2002.

22. Hugenholtz, C.H.; Barchyn, T.E.; Favaro, E.A. Formation of Periodic Bedrock Ridges on Earth. *Aeolian Res.* **2015**, *18*, 135–144. [[CrossRef](#)]
23. de Silva, S.L.; Spagnuolo, M.G.; Bridges, N.T.; Zimbelman, J.R. Gravel-Mantled Megaripples of the Argentinean Puna: A Model for Their Origin and Growth with Implications for Mars. *Bull. Geol. Soc. Am.* **2013**, *125*, 1912–1929. [[CrossRef](#)]
24. Foroutan, M.; Zimbelman, J.R. Mega-Ripples in Iran: A New Analog for Transverse Aeolian Ridges on Mars. *Icarus* **2016**, *274*, 99–105. [[CrossRef](#)]
25. Foroutan, M.; Steinmetz, G.; Zimbelman, J.R.; Duguay, C.R. Megaripples at Wau-an-Namus, Libya: A New Analog for Similar Features on Mars. *Icarus* **2019**, *319*, 840–851. [[CrossRef](#)]
26. Hugenholtz, C.H.; Barchyn, T.E. A Terrestrial Analog for Transverse Aeolian Ridges (TARs): Environment, Morphometry, and Recent Dynamics. *Icarus* **2017**, *289*, 239–253. [[CrossRef](#)]
27. Zimbelman, J.R.; Scheidt, S.P. Precision Topography of a Reversing Sand Dune at Bruneau Dunes, Idaho, as an Analog for Transverse Aeolian Ridges on Mars. *Icarus* **2014**, *230*, 29–37. [[CrossRef](#)]
28. Vriend, N.M.; Jarvis, P.A. Between a Ripple and a Dune. *Nat. Phys.* **2018**, *14*, 741–742. [[CrossRef](#)]
29. Sullivan, R.; Bridges, N.; Herkenhoff, K.; Hamilton, V.; Rubin, D. Transverse Aeolian Ridges (TARs) as Megaripples: Rover Encounters at Meridiani Planum, Gusev, and Gale. In Proceedings of the Eighth International Conference on Mars, Pasadena, CA, USA, 14–18 July 2014; Volume 1791, p. 1424.
30. Zimbelman, J.R. The Transition between Sand Ripples and Megaripples on Mars. *Icarus* **2019**, *333*, 127–129. [[CrossRef](#)]
31. Hugenholtz, C.H.; Barchyn, T.E.; Boulding, A. Morphology of Transverse Aeolian Ridges (TARs) on Mars from a Large Sample: Further Evidence of a Megaripple Origin? *Icarus* **2017**, *286*, 193–201. [[CrossRef](#)]
32. Zimbelman, J.R.; Foroutan, M. Dingo Gap: Curiosity Went Up a Small Transverse Aeolian Ridge and Came Down a Megaripple. *J. Geophys. Res. Planets* **2020**. [[CrossRef](#)]
33. Sullivan, R.; Kok, J.F.; Kutra, I.; Yizhaq, H. A Broad Continuum of Aeolian Impact Ripple Morphologies on Mars Is Enabled by Low Wind Dynamic Pressures. *J. Geophys. Res. Planets* **2020**, *125*, 1–39. [[CrossRef](#)]
34. Bagnold, R.A. *The Physics of Blown Sand and Desert Dunes*; Methuen: London, UK, 1941; ISBN 0486141195.
35. Parsons, A.J.; Abrahams, A.D. Geomorphology of desert environments. In *Geomorphology of Desert Environments*; Springer: Berlin/Heidelberg, Germany, 1994; pp. 3–12.
36. Middleton, G.V.; Southard, J.B. Mechanics of Sediment Transport. In *Society for Economic Paleontology and Mineralogy Short Course*; McMaster University: Hamilton, ON, USA, 1984; Volume 3.
37. Jakel, D. Die Bildung von Barchanen in Faya-Largeau/Rep. Du Tchad. *Z. Geomorphol.* **1980**, *24*, 141–159.
38. Kocurek, G.; Townsley, M.; Yeh, E.; Havholm, K.; Sweet, M.L. Dune and Dune-Field Development on Padre Island, Texas, with Implications for Interdune Deposition and Water-Table-Controlled Accumulation. *J. Sediment. Petrol.* **1992**, *62*, 622–635. [[CrossRef](#)]
39. Cooper, W.S. *Coastal Sand Dunes of Oregon and Washington*; Geological Society of America: Boulder, CO, USA, 1958; Volume 72, ISBN 0813710723.
40. Werner, B.T. Eolian Dunes: Computer Simulations and Attractor Interpretation. *Geology* **1995**, *23*, 1107–1110. [[CrossRef](#)]
41. Wiggs, G.F.S. Desert Dune Dynamics and the Evaluation of Shear Velocity: An Integrated Approach. *Geol. Soc. Spec. Publ.* **1993**, *72*, 37–46. [[CrossRef](#)]
42. Burkinshaw, J.R.; Illenberger, W.K.; Rust, I.C. Wind-Speed Profiles over a Reversing Transverse Dune. *Geol. Soc. Spec. Publ.* **1993**, *72*, 25–36. [[CrossRef](#)]
43. Lancaster, N. *Geomorphology of Desert Dunes*; Psychology Press: London, UK, 1995; ISBN 0415060931.
44. Mulligan, K.R. Velocity Profiles Measured on the Windward Slope of a Transverse Dune. *Earth Surf. Process. Landf.* **1988**, *13*, 573–582. [[CrossRef](#)]
45. Hunt, J.C.R.; Leibovich, S.; Richards, K.J. Turbulent Shear Flows over Low Hills. *Q. J. R. Meteorol. Soc.* **1988**, *114*, 1435–1470. [[CrossRef](#)]
46. Jackson, P.S.; Hunt, J.C.R. Turbulent Wind Flow over a Low Hill. *Q. J. R. Meteorol. Soc.* **1975**, *101*, 929–955. [[CrossRef](#)]
47. Zeman, O.; Jensen, N.O. Modification of Turbulence Characteristics in Flow over Hills. *Q. J. R. Meteorol. Soc.* **1987**, *113*, 55–80. [[CrossRef](#)]
48. Mason, P.J.; Sykes, R.I. Flow over an Isolated Hill of Moderate Slope. *Q. J. R. Meteorol. Soc.* **1979**, *105*, 383–395. [[CrossRef](#)]
49. Lancaster, N.; Nickling, W.G.; McKenna Neuman, C.K.; Wyatt, V.E. Sediment Flux and Airflow on the Stoss Slope of a Barchan Dune. *Geomorphology* **1996**, *17*, 55–62. [[CrossRef](#)]
50. Lancaster, N. Desert Dune Processes and Dynamics. *Arid Zone Geomorphol. Process Form Chang. Drylands* **2011**, *25*, 487–515. [[CrossRef](#)]
51. Parsons, D.R.; Wiggs, G.F.S.; Walker, I.J.; Ferguson, R.I.; Garvey, B.G. Numerical Modelling of Airflow over an Idealised Transverse Dune. *Environ. Model. Softw.* **2004**, *19*, 153–162. [[CrossRef](#)]
52. Weng, W.S.; Hunt, J.C.R.; Carruthers, D.J.; Warren, A.; Wiggs, G.F.S.; Livingstone, I.; Castro, I. Air flow and sand transport over sand-dunes. In *Aeolian Grain Transport*; Springer: Berlin/Heidelberg, Germany, 1991; pp. 1–22.
53. Walker, I.J.; Nickling, W.G. Dynamics of Secondary Airflow and Sediment Transport over and in the Lee of Transverse Dunes. *Prog. Phys. Geogr.* **2002**, *26*, 47–75. [[CrossRef](#)]
54. Frank, A.J.; Kocurek, G. Airflow up the Stoss Slope of Sand Dunes: Limitations of Current Understanding. *Geomorphology* **1996**, *17*, 47–54. [[CrossRef](#)]

55. Frank, A.; Kocurek, G. Toward a Model for Airflow on the Lee Side of Aeolian Dunes. *Sedimentology* **1996**, *43*, 451–458. [[CrossRef](#)]
56. Walker, I.J. Secondary Airflow and Sediment Transport in the Lee of a Reversing Dune. *Earth Surf. Process. Landf.* **1999**, *24*, 437–448. [[CrossRef](#)]
57. Reffet, E.; du Pont, S.C.; Hersen, P.; Douady, S. Formation and Stability of Transverse and Longitudinal Sand Dunes. *Geology* **2010**, *38*, 491–494. [[CrossRef](#)]
58. Gao, X.; Narteau, C.; Rozier, O. Development and Steady States of Transverse Dunes: A Numerical Analysis of Dune Pattern Coarsening and Giant Dunes. *J. Geophys. Res. F Earth Surf.* **2015**, *120*, 2200–2219. [[CrossRef](#)]
59. Yizhaq, H.; Ashkenazy, Y.; Tsoar, H. Why Do Active and Stabilized Dunes Coexist under the Same Climatic Conditions? *Phys. Rev. Lett.* **2007**, *98*, 98–101. [[CrossRef](#)]
60. Tsoar, H. Profiles Analysis of Sand Dunes and Their Steady State Signification. *Geogr. Ann.* **2007**, *67*, 47–59. [[CrossRef](#)]
61. Renwick, W.H. Equilibrium, Disequilibrium, and Nonequilibrium Landforms in the Landscape. *Geomorphology* **1992**, *5*, 265–276. [[CrossRef](#)]
62. Kocurek, G.A.; Havholm, K.G.; Deynoux, M.; Blakey, R.C. Amalgamated Accumulations Resulting from Climatic and Eustatic Changes, Akchar Erg, Mauritania. *Sedimentology* **1991**, *38*, 751–772. [[CrossRef](#)]
63. Lancaster, N.; Kocurek, G.; Singhvi, A.; Pandey, V.; Deynoux, M.; Ghienne, J.F.; Lô, K. Late Pleistocene and Holocene Dune Activity and Wind Regimes in the Western Sahara Desert of Mauritania: Reply. *Geology* **2003**, *31*, 991–994. [[CrossRef](#)]
64. Bai, Y.; Wang, N.; Liao, K.; Klenk, P. Geomorphological Evolution Revealed by Aeolian Sedimentary Structure in Badain Jaran Desert on Alxa Plateau, Northwest China. *Chin. Geogr. Sci.* **2011**, *21*, 267–278. [[CrossRef](#)]
65. Wolfe, S.A.; Huntley, D.J.; Ollerhead, J. Relict Late Wisconsinan Dune Fields of the Northern Great Plains, Canada. *Geogr. Phys. Quat.* **2004**, *58*, 323–336. [[CrossRef](#)]
66. Gardin, E.; Allemand, P.; Quantin, C.; Silvestro, S.; Delacourt, C. Dune Fields on Mars: Recorders of a Climate Change? *Planet. Space Sci.* **2012**, *60*, 314–321. [[CrossRef](#)]
67. Bristow, C.S.; Augustinus, P.C.; Wallis, I.C.; Jol, H.M.; Rhodes, E.J. Investigation of the Age and Migration of Reversing Dunes in Antarctica Using GPR and OSL, with Implications for GPR on Mars. *Earth Planet. Sci. Lett.* **2010**, *289*, 30–42. [[CrossRef](#)]
68. Kocurek, G. Interpretation of Ancient Eolian Sand Dunes. *Annu. Rev. Earth Planet. Sci.* **1991**, *19*, 43–75. [[CrossRef](#)]
69. Sharp, R.P. Wind Ripples. *The Journal of Geology* **1963**, *71*, 617–636. [[CrossRef](#)]
70. Kok, J.F.; Parteli, E.J.; Michaels, T.I.; Karam, D.B. The Physics of Wind-Blown Sand and Dust. *Rep. Prog. Phys.* **2012**, *75*, 106901. [[CrossRef](#)]
71. Goossens, D. Aeolian Dust Ripples: Their Occurrence, Morphometrical Characteristics, Dynamics and Origin. *Catena* **1991**, *18*, 379–407. [[CrossRef](#)]
72. Lämmel, M.; Meiwald, A.; Yizhaq, H.; Tsoar, H.; Katra, I.; Kroy, K. Aeolian Sand Sorting and Megaripple Formation. *Nat. Phys.* **2018**, *14*, 759–765. [[CrossRef](#)]
73. Milana, J.P. Largest Wind Ripples on Earth? *Geology* **2009**, *37*, 343–346. [[CrossRef](#)]
74. Yizhaq, H.; Katra, I.; Kok, J.F.; Isenberg, O. Transverse Instability of Megaripples. *Geology* **2012**, *40*, 459–462. [[CrossRef](#)]
75. Yizhaq, H.; Bel, G.; Silvestro, S.; Elperin, T.; Kok, J.F.; Cardinale, M.; Provenzale, A.; Katra, I. The Origin of the Transverse Instability of Aeolian Megaripples. *Earth Planet. Sci. Lett.* **2019**, *512*, 59–70. [[CrossRef](#)]
76. Yizhaq, H. A Simple Model of Aeolian Megaripples. *Phys. A Stat. Mech. Its Appl.* **2004**, *338*, 211–217. [[CrossRef](#)]
77. Yizhaq, H. A Mathematical Model for Aeolian Megaripples on Mars. *Phys. A Stat. Mech. Its Appl.* **2005**, *357*, 57–63. [[CrossRef](#)]
78. Isenberg, O.; Yizhaq, H.; Tsoar, H.; Wenkart, R.; Karnieli, A.; Kok, J.F.; Katra, I. Megaripple Flattening Due to Strong Winds. *Geomorphology* **2011**, *131*, 69–84. [[CrossRef](#)]
79. Katra, I.; Yizhaq, H.; Kok, J.F. Mechanisms Limiting the Growth of Aeolian Megaripples. *Geophys. Res. Lett.* **2014**, *41*, 858–865. [[CrossRef](#)]
80. Yizhaq, H.; Katra, I. Longevity of Aeolian Megaripples. *Earth Planet. Sci. Lett.* **2015**, *422*, 28–32. [[CrossRef](#)]
81. Lorenz, R.D.; Valdez, A. Variable Wind Ripple Migration at Great Sand Dunes National Park and Preserve, Observed by Timelapse Imaging. *Geomorphology* **2011**, *133*, 1–10. [[CrossRef](#)]
82. Sakamoto-Arnold, C.M. Eolian Features Produced by the December 1977 Windstorm, Southern San Joaquin Valley, California. *J. Geol.* **1981**, *89*, 129–137. [[CrossRef](#)]
83. Zimbelman, J.R.; Irwin, R.P.; Williams, S.H.; Bunch, F.; Valdez, A.; Stevens, S. The Rate of Granule Ripple Movement on Earth and Mars. *Icarus* **2009**, *203*, 71–76. [[CrossRef](#)]
84. Fenton, L.K.; Mellon, M.T. Thermal Properties of Sand from Thermal Emission Spectrometer (TES) and Thermal Emission Imaging System (THEMIS): Spatial Variations within the Proctor Crater Dune Field on Mars. *J. Geophys. Res. E Planets* **2006**, *111*. [[CrossRef](#)]
85. Presley, M.A.; Christensen, P.R. Thermal Conductivity Measurements of Particulate Materials 1. A Review. *J. Geophys. Res. E Planets* **1997**, *102*, 6535–6549. [[CrossRef](#)]
86. Lapotre, M.G.A.; Ewing, R.C.; Lamb, M.P.; Fischer, W.W.; Grotzinger, J.P.; Rubin, D.M.; Lewis, K.W.; Ballard, M.J.; Day, M.; Gupta, S.; et al. Large Wind Ripples on Mars: A Record of Atmospheric Evolution. *Science* **2016**, *353*, 55–58. [[CrossRef](#)]
87. Sullivan, R.; Arvidson, R.; Bell, J.F.; Gellert, R.; Golombek, M.; Greeley, R.; Herkenhoff, K.; Johnson, J.; Thompson, S.; Whelley, P.; et al. Wind-Driven Particle Mobility on Mars: Insights from Mars Exploration Rover Observations at “El Dorado” and Surroundings at Gusev Crater. *J. Geophys. Res.* **2008**, *113*, 1–70. [[CrossRef](#)]

88. Silvestro, S.; Fenton, L.K.; Vaz, D.A.; Bridges, N.T.; Ori, G.G. Ripple Migration and Dune Activity on Mars: Evidence for Dynamic Wind Processes. *Geophys. Res. Lett.* **2010**, *37*, 5–10. [[CrossRef](#)]
89. Chojnacki, M.; Banks, M.E.; Fenton, L.K.; Urso, A.C. Boundary Condition Controls on the High-Sand-Flux Regions of Mars. *Geology* **2019**, *47*, 427–430. [[CrossRef](#)] [[PubMed](#)]
90. Fenton, L.K.; Silvestro, S.; Kocurek, G. Transverse Aeolian Ridge Growth Mechanisms and Pattern Evolution in Scandia Cavi, Mars. *Front. Earth Sci.* **2021**, *8*, 1–17. [[CrossRef](#)]
91. McEwen, A.S.; Eliason, E.M.; Bergstrom, J.W.; Bridges, N.T.; Hansen, C.J.; Delamere, W.A.; Grant, J.A.; Gulick, V.C.; Herkenhoff, K.E.; Keszthelyi, L.; et al. Mars Reconnaissance Orbiter’s High Resolution Imaging Science Experiment (HiRISE). *J. Geophys. Res. E Planets* **2007**, *112*. [[CrossRef](#)]
92. ESRI ArcGIS Pro 2. 7. *Environmental Systems Research Institute ArcGIS Desktop*; ESRI: Redlands, CA, USA, 2020.
93. Bourke, M.C.; Wilson, S.A.; Zimbelman, J.R. The Variability of Transverse Aeolian Ridges in Troughs on Mars. In Proceedings of the Lunar and Planetary Science XXXIV, March, TX, USA, 17–21 March 2003; p. 2090.
94. Walker, I.J.; Hesp, P.A.; Davidson-Arnott, R.G.D.; Bauer, B.O.; Namikas, S.L.; Ollerhead, J. Responses of Three-Dimensional Flow to Variations in the Angle of Incident Wind and Profile Form of Dunes: Greenwich Dunes, Prince Edward Island, Canada. *Geomorphology* **2009**, *105*, 127–138. [[CrossRef](#)]
95. Hesp, P.A.; Smyth, T.A.G.; Nielsen, P.; Walker, I.J.; Bauer, B.O.; Davidson-Arnott, R. Flow Deflection over a Foredune. *Geomorphology* **2015**, *230*, 64–74. [[CrossRef](#)]
96. Walker, I.J.; Hesp, P.A. *Fundamentals of Aeolian Sediment Transport: Airflow over Dunes*; Elsevier Ltd.: Amsterdam, The Netherlands, 2013; Volume 11, ISBN 9780080885223.
97. Zimbelman, J.R.; Williams, S.H.; Johnston, A.K. Cross-Sectional Profiles of Sand Ripples, Megaripples, and Dunes: A Method for Discriminating between Formational Mechanisms. *Earth Surf. Process. Landf.* **2012**, *37*, 1120–1125. [[CrossRef](#)]
98. Ewing, R.C.; Peyret, A.P.B.; Kocurek, G.; Bourke, M. Dune Field Pattern Formation and Recent Transporting Winds in the Olympia Undae Dune Field, North Polar Region of Mars. *J. Geophys. Res. E Planets* **2010**, *115*, 1–25. [[CrossRef](#)]
99. Swanson, T.; Mohrig, D.; Kocurek, G.; Perillo, M.; Venditti, J. Bedform Spurs: A Result of a Trailing Helical Vortex Wake. *Sedimentology* **2018**, *65*, 191–208. [[CrossRef](#)]
100. Mason, J.; Cardenas, B.T.; Day, M.D.; Daniller-Varghese, M.; Brothers, S.C.; Kocurek, G.; Mohrig, D. Pattern Evolution and Interactions in Subaqueous Dune Fields: North Loup River, Nebraska, U.S.A. *J. Sedimentary Res.* **2020**, *90*, 1734–1746. [[CrossRef](#)]
101. Nagle-Mcnaughton, T.; McClanahan, T.; Scuderi, L. PlaNet: A Neural Network for Detecting Transverse Aeolian Ridges on Mars. *Remote Sens.* **2020**, *12*, 3607. [[CrossRef](#)]
102. Golombek, M.; Robinson, K.; McEwen, A.; Bridges, N.; Ivanov, B.; Tornabene, L.; Sullivan, R. Constraints on Ripple Migration at Meridiani Planum from Opportunity and HiRISE Observations of Fresh Craters. *J. Geophys. Res. E Planets* **2010**, *115*, 1–34. [[CrossRef](#)]
103. Goudge, T.A.; Milliken, R.E.; Head, J.W.; Mustard, J.F.; Fassett, C.I. Sedimentological Evidence for a Deltaic Origin of the Western Fan Deposit in Jezero Crater, Mars and Implications for Future Exploration. *Earth Planetary Sci. Lett.* **2017**, *458*, 357–365. [[CrossRef](#)]